Research Article | Vol. 27, No. 26 / 23 December 2019 / Optics Express 38451
Optics EXPRESS

Asymmetric valley polarization and photoluminescence in MoS_2/MoO_3 heterostructure

WEN-BO SHI,[1] JIE HE,[1] QING-XUAN LI,[1] XI-CHAO SHE,[1] DI WANG,[1] HAO JING,[1] RUI-LI ZHANG,[1,3] JIN-ZHU ZHAO,[2] RU-WEN PENG,[1,4] HU XU,[2] AND MU WANG[1,5]

[1]*National Laboratory of Solid State Microstructures, School of Physics, and Collaborative Innovation Center of Advanced Microstructures, Nanjing University, Nanjing 210093, China*
[2]*Department of Physics and Institute for Quantum Science and Engineering, Southern University of Science and Technology, Shenzhen 518055, China*
[3]*rlzhang@nju.edu.cn*
[4]*rwpeng@nju.edu.cn*
[5]*muwang@nju.edu.cn*

Abstract: We investigate circularly polarized photoluminescence (PL) in the MoS_2/MoO_3 heterostructure, which was fabricated by transferring MoS_2 monolayer to cover the MoO_3 few layers on the SiO_2/Si substrate. It is shown that the PL with the same helicity as the excitation light is dominant due to the inherent chiral optical selectivity, which allows exciting one of the valleys in MoS_2 monolayer. The degree of polarization (DP), which characterizes the intensity difference of two chiral components of PL, is unequal for the right-handed and left-handed circularly polarized excitations in the MoS_2/MoO_3 heterostructure. This effect is different from the one in pristine MoS_2. Our Raman spectra results together with *ab* initio calculations indicate the p-doped features of the MoS_2 when it covers the MoO_3 layers. Thus the possible explanation of the unequal DP is that the p-doping process generates a built-in voltage and therefore brings the difference of electron-hole overlaps between K and K′ valleys. Namely the asymmetric valley polarization may be obtained in the MoS_2/MoO_3 heterostructure. Consequently, the circularly polarized PL caused by the electron-hole recombination at K and K′ valleys manifests unequal DP for the right-handed and left-handed helix excitations. This asymmetric effect is further enhanced by decreasing the temperature in the MoS_2/MoO_3 heterostructure. Our investigation provides a unique platform for developing novel two-dimensional valleytronic devices.

1. Introduction

Since initial proposal of the valley index as potential information carriers by Gunawan *et al.* in 2006 [1], considerable attention has been paid to the materials with the valley degree of freedom (DOF) [2–5]. Due to their unique band structures, two-dimensional (2D) transition metal dichalcogenides (TMDs) are considered as a group of promising candidates with the common formula MX_2 (MoS_2, $MoSe_2$, WS_2, WSe_2, and so forth) [6–12]. Specifically, there are two inequivalent valleys in the band structure of monolayer TMDs at the boundary of the Brillouin zone, K and K′ points, with opposite spin splitting, *i.e.*, the inherent spin and valley locking, caused by strong spin-orbit coupling and the inversion symmetry breaking [13]. Carriers in the two valleys are associated with opposite values of Berry curvature, and experience effective magnetic fields with equal magnitudes but opposite signs [13]. When an in-plane electric field is applied, valley-polarized carriers experience opposite Lorentz-like forces and flow to opposite transverse edges, *i.e.*, valley Hall effect, which has been demonstrated in monolayer MoS_2 by using electric readout method [14]. Such effective magnetic fields can also lead to

#381995 https://doi.org/10.1364/OE.27.038451
Journal © 2019 Received 5 Nov 2019; revised 26 Nov 2019; accepted 27 Nov 2019; published 18 Dec 2019
Corrected: 13 January 2020

Optics EXPRESS

valley-dependent optical selection rules where the inter-band transitions in the vicinity of the K (K′) point couple exclusively to right (left)-handed circularly polarized light σ^+ (σ^-) [15]. Circularly polarized photoluminescence (PL) in monolayer MoS_2 has been measured by Zeng *et al.* [16]. They found that the right (left)-handed circularly polarized excitation generates right (left)-handed luminescence. The PL spectra display a symmetric polarization for excitations with opposite helicities, indicating the symmetric valley polarization in MoS_2 monolayer. Recently, great efforts have been devoted to control the properties of optics by coupling a TMD monolayer to plasmonic nanostructures [17–19]. Sun *et al.* demonstrated that, by coupling a MoS_2 monolayer to the designed metasurface, photons with opposite helicity can be guided to different directions [20].

Precise controlling and manipulating the valley polarization is the fundamental basis for the application of valley index as information carriers. The strategies of directly applying perpendicular magnetic fields [21], generating pseudomagnetic fields by intense circularly polarized optical pulses [22], and inducing a magnetic exchange field through magnetic proximity effect [23] in monolayer TMDs, have been used to achieve this goal. On one hand, under the magnetic fields, the energy degeneracy of valleys is lifted due to the time-reversal symmetry breaking, leading to the change of valley polarization. Consequently the valley-dependent circularly polarized PL can be manipulated by tuning external magnetic fields [21]. On the other hand, by injecting specific spin-polarized charge carriers to populate K (or K′) valley in monolayer TMDs, valley-polarized electroluminescence (EL) was captured because of the spin-valley locking [24,25]. Valley-polarized EL has also been realized by Zhang *et al.* via an in-plane electric field giving rise to valley overlap polarization (VOP) in MoS_2, $MoSe_2$, and WSe_2 [26]. Recently, Yang *et al.* demonstrated the electrically tunable chiral EL from WS_2 by constructing a p-i-n heterojunction [27]. Motivated by these researches, we propose that the valley polarization and circularly polarized PL should also be altered in MoS_2 with specific heterostructures.

In this work, we investigate circularly polarized photoluminescence (PL) in the MoS_2/MoO_3 heterostructure fabricated by transferring MoS_2 monolayer to cover the MoO_3 few layers on the SiO_2/Si substrate. By measuring the Raman spectra together with *ab* initio calculations, it is found that the MoS_2 was p-doped in the MoS_2/MoO_3 heterostructure. This phenomenon comes from the carriers transferring between MoS_2 and MoO_3 layers due to their specific band structures. This process may generate a built-in voltage which leads to the difference of electron-hole overlaps between the K and K′ valleys. Thus, the circularly polarized PL caused by the electron-hole recombination at K and K′ valleys performs different degree of polarization (DP) for the right and left-handed helix. Consequently, asymmetric valley polarization and the unequal DP for the right and left-handed circularly polarized PL are obtained in the MoS_2/MoO_3 heterostructure. This asymmetric effect is further enhanced by decreasing the temperature in the system. Our investigation provides an opportunity for developing valleytronics and novel two-dimensional optoelectronic devices.

2. Fabrication and p-doping of MoS_2/MoO_3 heterostructure

The configuration of the MoS_2/MoO_3 heterostructure on SiO_2/Si substrate is schematically illustrated in Fig. 1(a). The whole structure consists of a MoS_2 monolayer, the MoO_3 few layers, and the SiO_2/Si substrate from top to bottom. The 514 nm laser (Stabilite 2018-RM, Spectra-Physics) is used to excite the sample. Our measurements were carried out in an optical microscope (BX51, Olympus) by using a ×100 objective lens (NA = 0.9, Olympus) to focus laser beams onto the sample surface. The combination of quarter waveplates and linear polarizers were used to generate circularly polarized excitation beams and to analyze the degree of PL circular polarization. The exciting light was suppressed by a long pass filter before the signal enters the spectrograph (Acton SP2500, Princeton Instrument) in order to avoid the influence

Optics EXPRESS

of the noise from pumping light [as shown in Fig. 1(b)]. In the experiments, the MoS_2 and MoO_3 layers were grown by chemical vapor deposition (CVD) method [17] and ambient pressure physical vapor deposition (APPVD) [28], respectively. Specifically, the MoO_3 sheets were grown on the mica firstly by vaporizing the MoO_3 powder from room temperature to 680°C within 60 min. The distance between the MoO_3 powder (Alfa Aesar, purity 99.95%) and the freshly cleaved mica is 30 cm in size. The MoS_2 monolayers were grown on a SiO_2/Si substrate by heating the sulfur powder and the substrate to 140°C and 780°C, respectively, within 25 min. The sulfur powder (Aladdin, purity 99.95%) was positioned 45 cm away from the substrate. A flow rate 50 sccm N_2 was used as the carrier gas. The as-grown MoO_3/mica was spin-coated with PMMA at 2000rpm for one minute. The edge of PMMA films was scraped off. Then the PMMA/MoO_3/mica was immersed in deionized water, leading to the PMMA/MoO_3 films delaminate from the mica substrate. And the PMMA/MoO_3 film was collected by the SiO_2/Si substrate. Finally, the heterostructure sample is fabricated by transferring MoS_2 monolayer (about 0.8 nm) to cover the MoO_3 few layers (about 16 nm) on the SiO_2/Si substrate in the same way. Figure 1(c) shows the optical image of prepared MoS_2/MoO_3 heterostructure. The white scale bar is 2μm. The fabricated MoS_2 monolayer and MoO_3 few layers are identified by the mapping images of Raman shift [as shown in the insets of Fig. 1(c)], which were obtained by scanning the region of heterostructure and extracting Raman shift signals of 403 rel cm^{-1} and 815 rel cm^{-1}, respectively.

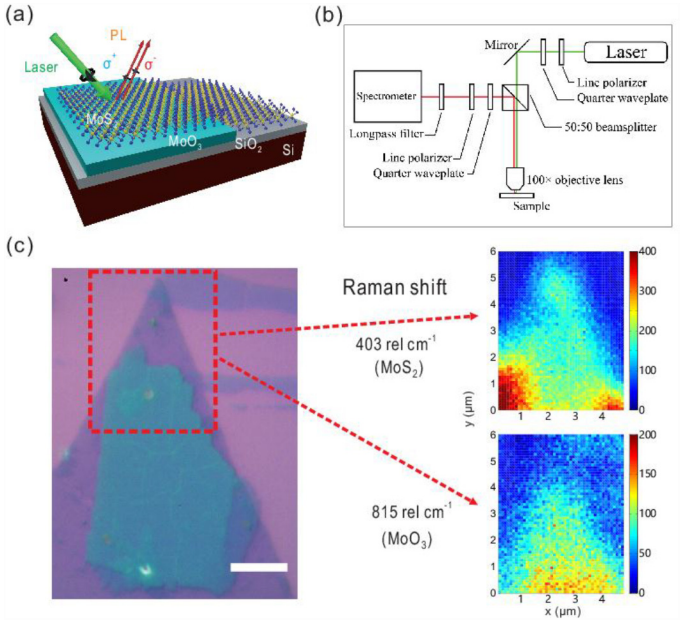

Fig. 1. (a) Schematic image of the MoS_2/MoO_3 heterostructure. It consists of a MoS_2 monolayer, the MoO_3 few layers, and the SiO_2/Si substrate from top to bottom. The 514 nm laser is used to excite the sample. (b) Diagrammatic sketch of measurements. (c) Optical image of MoS_2/MoO_3 heterostructure. The scale bar is 2μm. The insets show the Raman shift of 403 rel cm^{-1} (from MoS_2) and 815 rel cm^{-1} (from MoO_3), respectively.

In order to understand how the MoS_2 is modified after it covers the MoO_3 few layers, Raman shifts of both pristine MoS_2 and MoS_2/MoO_3 heterostructure have been measured. The solid blue line in Fig. 2(a) illustrates the Raman shift of pristine MoS_2. It is obvious that two Raman peaks, *i.e.*, in-plane $E^1{}_{2g}$ and out-of-plane A_{1g} modes, were observed at 384 rel cm^{-1} and 403 rel cm^{-1}, respectively. The frequency difference between the two modes is 19 rel cm^{-1}. This indicates

Optics EXPRESS

the monolayer nature of the CVD-grown MoS_2. In contrast, the peak position of A_{1g} modes is blue-shifted in the MoS_2/MoO_3 heterostructure [see the red dashed line in Fig. 2(a)]. Blue shift of the A_{1g} peak has been reported as an evidence of p-doping [29]. Therefore, the MoS_2 is p-doped after it covers the MoO_3 few layers forming the MoS_2/MoO_3 heterostructure. On the other hand, the normalized PL spectra of both pristine MoS_2 and MoS_2/MoO_3 heterostructure have been measured for comparison. As shown in Fig. 2(b), there are two PL peaks both for pristine MoS_2 [solid blue line in Fig. 2(b)] and the MoS_2/MoO_3 heterostructure [solid red line in Fig. 2(b)]. The two PL peaks represent two kinds of excitons: A exciton and B exciton. Notice that peak intensity of A exciton in the MoS_2/MoO_3 heterostructure is enhanced and blue shifted compared with that in the pristine MoS_2. The enhancement of PL intensity might be related to the phase-space filling effect [30–31]. Specifically, the MoS_2 sample was intrinsic n-doped due to the S vacancy in CVD-grown MoS_2 monolayer [32]. The majority carriers of electron may render part of the phase space unavailable for exciton formation. The transferring of holes from MoO_3 layer to MoS_2 layer can lead to the dedoping of monolayer n-doped MoS_2. Thus the PL from MoS_2/MoO_3 heterostructure is larger than that from pristine MoS_2. The similar results have been demonstrated in gate-tuned PL of monolayer MoS_2 in which the PL was enhanced due to the injection of holes [33]. In addition, the peak intensity ratio between A and B excitons in the MoS_2/MoO_3 heterostructure is larger than that in the pristine MoS_2 [as shown in Fig. 2(b)]. These features confirm the process of p-doping of MoS_2 in the MoS_2/MoO_3 heterostructure [29]. To clarify this p-doping process, the band diagrams of MoS_2 and MoO_3 layers are illustrated in Fig. 2(c). Obviously, there is a large band offset between MoS_2 and MoO_3 layers due to their different band gaps [34]. The electrons in the conduction band of MoS_2 are apt to transfer to the MoO_3 layer, and holes in the valence band of MoO_3 prefer to transfer to MoS_2 layer. Therefore, the charge transfer process that results in the p-doping of MoS_2 is reasonable. Notice that the conduction band minimum (CBM) and the valence band maximum (VBM) are located in different layers. It is possible that the photoexcited electrons and holes localize in the band edges in the different layers after rapid relaxation. Such bound electron-hole pairs are known as interlayer excitons which can decrease the intralayer PL signal from individual TMD monolayers [35]. However, the interlayer excitons are highly susceptible to the strength of the interlayer interaction between the two constituent layers. The presence of the adsorbates and residuals formed at the interface can reduce the degree of coupling between the two layers leading to the unavailable of the interlayer exciton. In our experiments, we did not observe the interlayer PL signal, and the PL of the MoS_2/MoO_3 heterostructure mainly originated from the neutral excitons in monolayer MoS_2 [as shown in the Fig. 2(b)]. Then the mechanism that the interlayer excitons decrease the intralayer PL signal can be ruled out in our system.

Furthermore, we studied the electronic state in the MoS_2/MoO_3 heterostructure based on density-functional theory [36–38]. The *ab* initio calculated results show that the electron cloud is distorted in the interface region comparing to the ones in original free standing MoS_2 and clean MoO_3 substrate. As the charge density difference shows, displayed in Fig. 2(d), electrons tend to accumulate in the interface, close to the MoO_3 substrate, away from monolayer MoS_2. By using the Bader charge analysis, we noticed that the distribution of valence electrons of MoO_3 substrate is altered near the interface [see Figs. 2(e), 2(f), and Table 1]. These phenomena are confirmed in both $p\left(2\sqrt{3}\times 5\right)$ and $p(6\times 6)$ MoS_2 supercell models [39–43]. Based on the theoretical results, it is estimated that the asymmetric PL for the right- and left-handed helix excitations is mainly originated from the distortion of electronic state due to the interface of the MoS_2/MoO_3 heterostructure. The coupling between MoS_2 and MoO_3 layers distorted the original electron cloud by weakly accumulating them in the interface region, acting as a p type doping in monolayer MoS_2. The corresponding p-doping is estimated at the same level of the electric gating and chemical adsorption doping effect [44,45]. This type of distortion breaks the original symmetry of our sample and therefore induces the different responds to incident

Optics EXPRESS

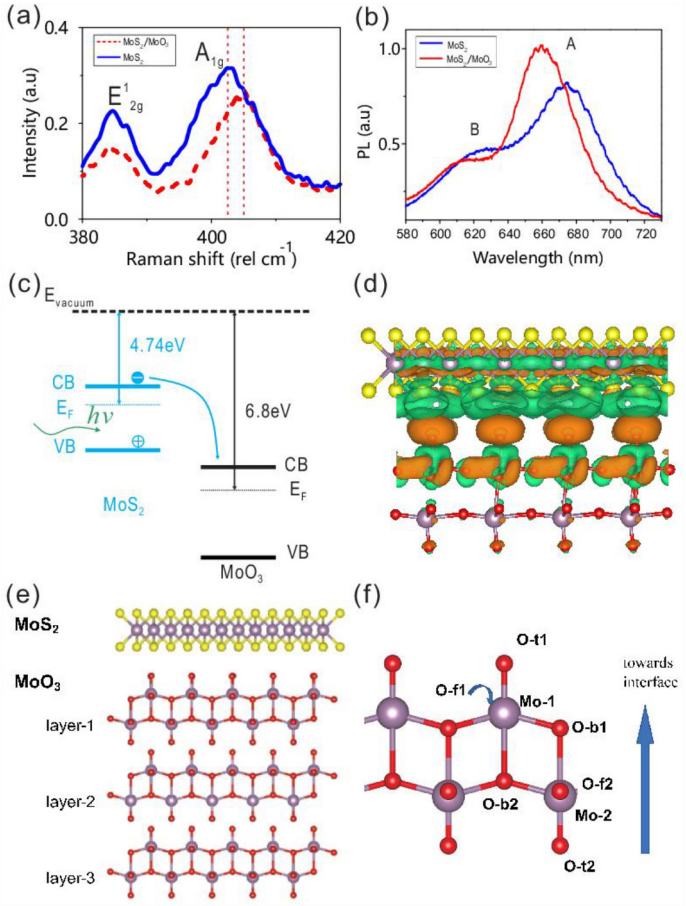

Fig. 2. (a) Raman shift of pristine MoS_2 and MoS_2/MoO_3 heterostructure. There is a blue shift of A_{1g} peak in MoS_2/MoO_3 heterostructure, which is the evidence of p-doping of monolayer MoS_2. (b) PL signal of pristine MoS_2 and MoS_2/MoO_3 heterostructure. The increased peak intensity of A exciton and the increased peak intensity ratio between A and B exciton confirm the p-doping of MoS_2 in the MoS_2/MoO_3 heterostructure. (c) Band structure of MoS_2/MoO_3 heterostructure. After absorbing the energy of a photon, electrons in conduction band of MoS_2 can transfer to MoO_3 layer and the hole in valence band is left. This process results the in-plane voltage in the heterostructure. (d) Charge density difference in a unit cell of MoS_2/MoO_3 heterostructure. The isosurface value is set to be 0.00015e/bohr^3. Orange and green color represent for the electron accumulation and depletion, respectively. The atoms with light purple, yellow, and red color are Mo, S, and O, respectively. (e) The scheme of p(6×6) MoS_2 supercell on the three layers p(4×5) MoO_3 supercell substrate. Each layer of MoO_3 substrate is labeled. (f) The labeling for atoms in each MoO_3 layer.

Optics EXPRESS

light with opposite chirality. It is worth to mention that the phenomena discussed above are very weak in amplitude, for both charge density difference and Bader charge data, since only very tiny electrons are able to transfer through the interface of the heterostructure.

Table 1. The distribution of valence electrons in MoO_3 substrates obtained from Bader charge analysis of the p(6×6) MoS_2 supercell on the three layers p(4×5) MoO_3 supercell substrate as it is shown in Fig. 2(e) and Fig. 2(f). The numbers of the atoms close to the interface region are different with the ones in the rest part of the substrate and are highlighted in red colour.

	Mo-1	*Mo-2*	*O-t1*	*O-t2*	*O-b1*	*O-b2*	*O-f1*	*O-f2*
layer-1	3.68	3.66	6.66	6.59	6.99	6.99	6.77	6.76
layer-2	3.66	3.65	6.59	6.59	6.99	6.99	6.76	6.76
layer-3	3.66	3.66	6.59	6.57	6.99	6.99	6.75	6.77

Particularly, after the excitation with the laser, the electrons are promoted from the valence band of MoS_2 to the conduction band. These excited electrons diffuse to the vicinities, and eventually populate the MoO_3 layer. This charge transfer process results in the p-doping of MoS_2. However, the MoS_2 pristine layer is intrinsic n-doping [46]. Therefore, it is p-doped in some regions while it is n-doped in the other regions in the same plane. As a result, the in-plane voltage should be generated in the MoS_2/MoO_3 heterostructure. The possible orientation of the in-plane electric field can be evaluated based on the observed PL spectra. It has been demonstrated that the degree of circular polarized electroluminescence is quite sensitive to the relative angle between the crystal orientation and the field direction in TMDs [26–27]. If the orientation of electric field is along the zigzag side of MoS_2, and from Γ to K' in the reciprocal space, the right-handed circular component is stronger than the left one. On the contrary, the left-handed circular component is stronger than the right one when the orientation of electric field is from Γ to K in the reciprocal space. The reason is that the carrier distribution in TMDs are intrinsically anisotropic due to trigonal warping [47], and the built-in electric field can lead to the shift of electron and hole distributions toward opposite directions. This process introduces different overlaps of electron-hole distributions in the momentum space between the K and K′ valleys. That is to say that the asymmetric valley polarization may happen in the MoS_2/MoO_3 heterostructure.

3. Circularly polarized photoluminescence in MoS_2/MoO_3 heterostructure

The asymmetric valley polarization can be determined through circularly polarized PL in the MoS_2/MoO_3 heterostructure. In the experiments, we have used right-handed circular polarized light (σ^+) to excite the sample, and then analyzed the PL signal by σ^+ and σ^- resolved detection, respectively. Similarly, left-handed polarized light (σ^-) was used to excite the sample, and the PL signal was analyzed by σ^+ and σ^- resolved detection, respectively. Figures 3(a)–3(b) and 3(d)–3(e) show the polarization resolved PL spectra of pristine MoS_2 and the MoS_2/MoO_3 heterostructure, respectively. Here, $\sigma^+-\sigma^\pm$ indicates the $\sigma^\pm$ resolved spectra with σ^+ excitation, and $\sigma^--\sigma^\pm$ denotes the $\sigma^\pm$ resolved spectra with σ^- excitation. It is demonstrated in Figs. 3(a) and 3(b), the intensity of $\sigma^--\sigma^-$ is stronger than that of $\sigma^--\sigma^+$, and the intensity of $\sigma^+-\sigma^+$ is stronger than that of $\sigma^+-\sigma^-$ at an arbitrary wavelength in the pristine MoS_2. That means the left-handed circularly polarized PL is dominant with left-handed circularly polarized excitation while the right-handed circularly polarized PL is dominant with right-handed circularly polarized excitation. Moreover, the contour between the curves of $\sigma^--\sigma^-$ and $\sigma^--\sigma^+$ is much alike to that between $\sigma^+-\sigma^+$ and $\sigma^+-\sigma^-$ [as shown in Figs. 3(a) and 3(b)]. The reason is that the K and K′ valleys are energetically degenerate although they have opposite spin splitting in the pristine MoS_2. As a consequence, the PL with the helicity following that of the excitation light is dominant, and the intensity difference between the two chiral components is equal at an

Optics EXPRESS

arbitrary wavelength for the right and left-handed circularly polarized excitation. The results coincide with the valley contrasting selection rule in the pristine MoS_2. On the other hand, we have measured the circularly polarized PL in the MoS_2/MoO_3 heterostructure. Obviously, the intensity of $\sigma^- - \sigma^-$ is stronger than or equal to that of $\sigma^- - \sigma^+$, and the intensity of $\sigma^+ - \sigma^+$ is stronger than that of $\sigma^+ - \sigma^-$ at an arbitrary wavelength [as shown in Figs. 3(d) and 3(e)]. Interestingly, it is noted that the spacing between $\sigma^- - \sigma^-$ and $\sigma^- - \sigma^+$ is reduced while the spacing between $\sigma^+ - \sigma^+$ and $\sigma^+ - \sigma^-$ is enhanced in the MoS_2/MoO_3 heterostructure compared with that in the pristine MoS_2. It implies that the MoS_2/MoO_3 heterostructure is in favor of right-handed circularly polarized PL from the K valley of MoS_2. The possible explanation is that the p-doping of MoS_2 in the MoS_2/MoO_3 heterostructure causes the emergence of a built-in voltage which can shift the overlaps of electron-hole distribution at K and K′ valleys in momentum space. When the orientation of built-in electric field is from Γ to K' in the reciprocal space, the right-handed circular component is stronger than the left one [26]. Specifically, the asymmetric valley polarization is obtained which impacts the electron-hole recombination in the K and K′ valleys [as shown in the insets of Figs. 3(c) and 3(f)]. As a result, the intensity difference between the two chiral components of PL is unequal for the right and left-handed circularly polarized excitation in the MoS_2/MoO_3 heterostructure. Particularly, the MoS_2/MoO_3 heterostructure is in favor of right-handed circularly polarized PL from the K valley of MoS_2.

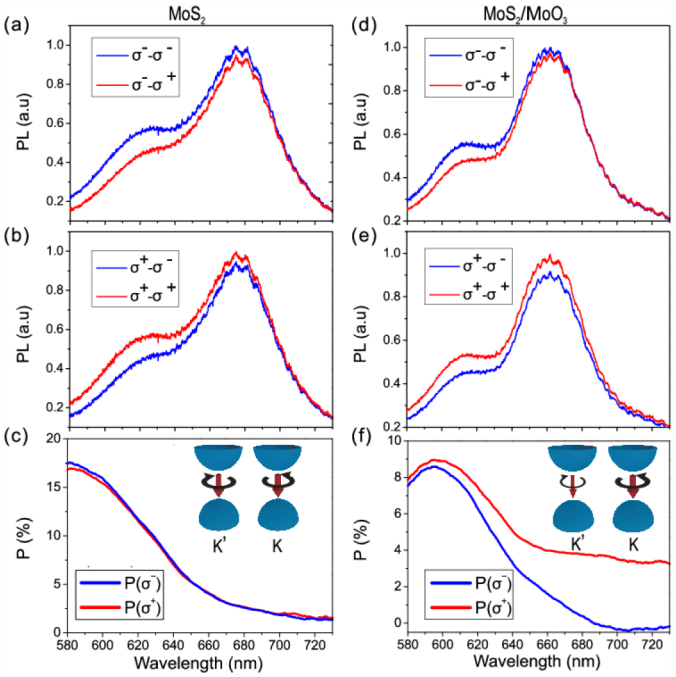

Fig. 3. σ^- and σ^+ detected PL signal of pristine MoS_2 with (a) σ^- excitation (b) σ^+ excitation. σ^+ and σ^- detected PL signal of MoS_2/MoO_3 heterostructure with (d) σ^- excitation (e) σ^+ excitation. DP of PL with σ^- (P (σ^-)) and σ^+ (P (σ^+)) excitation in (c) pristine MoS_2 and (f) MoS_2/MoO_3 heterostructure. Obviously, P (σ^-) is unequal to P (σ^+) in the MoS_2/MoO_3 heterostructure. The inset of (c) shows the electron-hole recombination when the K′ and K valleys are symmetric polarized in pristine MoS_2, and the inset of (f) shows the electron-hole recombination when the K′ and K valleys are asymmetric polarized in the MoS_2/MoO_3 heterostructure.

Optics EXPRESS

For the sake of clarity, the DPs of PL were defined as $P(\sigma^-) = [I(\sigma^-) - I(\sigma^+)]/[I(\sigma^-) + I(\sigma^+)]$ and $P(\sigma^+) = [I(\sigma^+) - I(\sigma^-)]/[I(\sigma^-) + I(\sigma^+)]$ when the MoS_2/MoO_3 heterostructure was excited by σ^- and σ^+, respectively. $I(\sigma^\pm)$ indicates the intensity of detected $\sigma^\pm$. It is found that the curves of $P(\sigma^-)$ and $P(\sigma^+)$ are almost coincided with each other in the pristine MoS_2 [as shown in Fig. 3(c)]. The reason is that the contour between $\sigma^- - \sigma^-$ and $\sigma^- - \sigma^+$ is alike to that between $\sigma^+ - \sigma^+$ and $\sigma^+ - \sigma^-$ due to the spin-valley locking and the energetic degeneracy of K and K′ valleys in the pristine MoS_2. However, the curves of $P(\sigma^+)$ and $P(\sigma^-)$ are separated, and $P(\sigma^+)$ is larger than $P(\sigma^-)$ at an arbitrary wavelength in the MoS_2/MoO_3 heterostructure [as shown in Fig. 3(f)]. This feature comes from the fact that the intensity difference between $\sigma^+ - \sigma^+$ and $\sigma^+ - \sigma^-$ is larger than that between $\sigma^- - \sigma^-$ and $\sigma^- - \sigma^+$ because of the asymmetric valley polarization [as shown in Figs. 3(d) and 3(e)]. Possibly, the overlaps of electron-hole distribution at K and K′ valleys are shifted in MoS_2 when it covers the MoO_3 few layers to form the MoS_2/MoO_3 heterostructure. Therefore, the PL caused by electron-hole recombination shows unequal DP for the right and left-handed circularly polarized excitation [as shown in the inset of Figs. 3(c) and 3(f)]. The experiment suggests that the MoS_2/MoO_3 heterostructure is in favor of right-handed circularly polarized PL. Namely $P(\sigma^+)$ is larger than $P(\sigma^-)$ at an arbitrary wavelength in the MoS_2/MoO_3 heterostructure.

It is worthwhile to verify the repeatability of the above properties. We have fabricated several samples of MoS_2/MoO_3 heterostructures and surveyed their circularly polarized PL. As shown in Fig. 4, there are several prominent features as follows. First, the profiles of $P(\sigma^+)$ (or $P(\sigma^-)$) are somewhat distorted when we choose different samples [as shown in Figs. 4(a)–4(d)]. Second, the lines of $P(\sigma^+)$ and $P(\sigma^-)$ are separated for the same sample. This feature may originate from the asymmetric valley polarization in the MoS_2/MoO_3 heterostructures. A possible mechanism is that the overlaps of electron-hole distribution at K and K′ valleys are different which can influence the electron-hole recombination. Consequently, the DP of PL is unequal for the right and left-handed circularly polarized excitations. Third, the line of $P(\sigma^+)$ is above that of $P(\sigma^-)$ for each sample, i.e., the MoS_2/MoO_3 heterostructure is in favor of right-handed circularly polarized PL. The reason is that the defects or disorders might be introduced during the sample fabrication process. The component of in-plane electric field that supports $P(\sigma^+)<P(\sigma^-)$ might be blocked which make the right-handed polarization preferred to the opposite helicity in the MoS_2/MoO_3 heterostructure. Similar phenomenon has also been found in [26]. Therefore, the features of asymmetric valley polarization and unequal DP of PL are universal in MoS_2/MoO_3 heterostructures.

It is interesting to investigate the DP of PL by changing the excitation wavelength and the power of excitation laser. As shown in Figs. 5(a) and 5(b), the profiles of $P(\sigma^+)$ (or $P(\sigma^-)$) are somewhat distorted when the excitation wavelength is changed. For the same excitation wavelength, the lines of $P(\sigma^+)$ and $P(\sigma^-)$ are separated. However, there isn't distinct variation for the gap between $P(\sigma^+)$ and $P(\sigma^-)$ by changing the excitation wavelengh. This effect agrees with the previous report in [48] that the excitation wavelength doesn't impact the electron transfer in MoS_2 based heterojunction. On the other hand, the DP of PL can be tuned by the input power of excitation. It is found that the gap between lines of $P(\sigma^+)$ and $P(\sigma^-)$ is enhanced by increasing the power of extitaion laser [as shown in Figs. 5(b)–5(d)]. The reason is that excitation laser with stronger power generates more excited electrons from the valence band of MoS_2 to the conduction band. These excited electrons diffuse to the vicinities, and eventually populate the MoO_3 layer. As a result, the electric field in heterostructure is enhanced by increasing the power of excitation laser, which can lead to the enlargement of the difference between $P(\sigma^+)$ and $P(\sigma^-)$. Therefore, the DP of PL can be enhanced by incresing the power of excitation laser in the MoS_2/MoO_3 heterostructures.

Figure 6 displays the temperature dependence of DP of the circularly polarized PL in the MoS_2/MoO_3 heterostructure. The liquid helium cryostat (ST-500-UC, JANIS) has been utilized

Optics EXPRESS

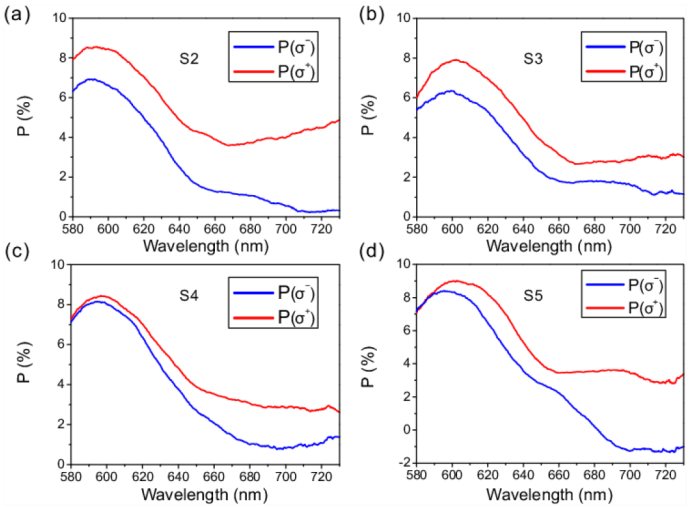

Fig. 4. (a)–(d) DP of PL with σ^- (P (σ^-)) and σ^+ (P (σ^+)) excitation in different MoS_2/MoO_3 heterostructure samples (S2-S5).

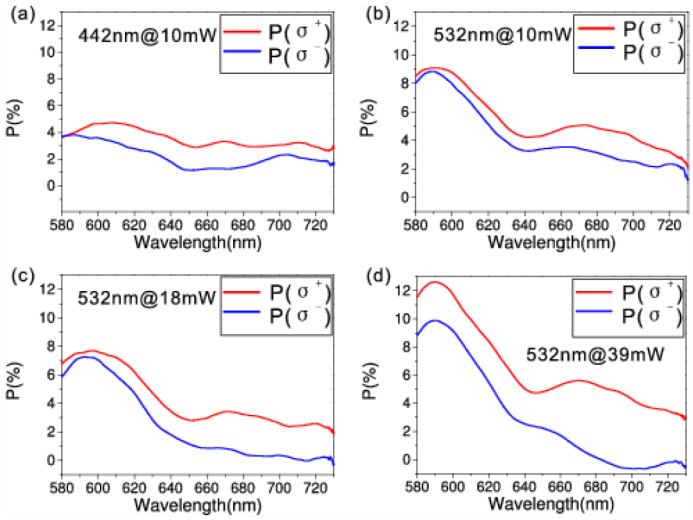

Fig. 5. DP of PL with σ^- (P (σ^-)) and σ^+ (P (σ^+)) excitation at different excitation wavelength and power of excitation laser: (a) 442 nm and 10 mW (MDL-III—442-30, CNILaser); (b) 532 nm and 10mW (MGL-H-532-1, CNILaser); (c) 532 nm and 18 mW; (d) 532 nm and 39 mW, respectively.

Optics EXPRESS

to approach the temperature as low as 4.8 K [49]. Here, the sample is different from the one used in Fig. 3(f). We have measured the circularly polarized PL at two different temperatures: 4.8 K and 270 K. It is shown in Figs. 6(a) and 6(b) that the curves of $P(\sigma^+)$ and $P(\sigma^-)$ are misaligned, and the curve of $P(\sigma^+)$ is above that of $P(\sigma^-)$ at each temperature. The gap between the curves of $P(\sigma^+)$ and $P(\sigma^-)$ at 270 K is smaller than that at 4.8 K [as shown in Fig. 6(c)]. This feature can be understood in terms of two competing factors: the recombination rate of the electron-hole and the transferring rate of electrons from MoS_2 layer to MoO_3 layer forming p-doping MoS_2. At low temperature, the PL has a much longer lifetime, and the recombination rate of electrons-holes in MoS_2 is smaller which benefits the amplification of the gap between $P(\sigma^+)$ and $P(\sigma^-)$. The other reason is that there is more phonon scattering at higher temperature, which hinders the electron transfer from MoS_2 to MoO_3 layers forming p-doping MoS_2. This procedure doesn't benefit the amplification of the gap between $P(\sigma^+)$ and $P(\sigma^-)$. However, the phonon scattering is unlikely to hinder electron transfer significantly since the offset between conduction bands of MoS_2 and MoO_3 is as large as ~2 eV illustrated in Fig. 2(c). Therefore, at lower temperature, the recombination rate is smaller while the electron transferring rate is not affected much, leading to the increased gap between $P(\sigma^+)$ and $P(\sigma^-)$.

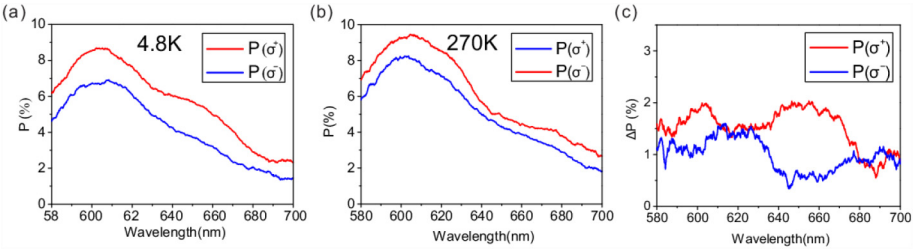

Fig. 6. (a) DP measured at 4.8 K. (b) DP measured at 270 K. The difference between P (σ^+) and P (σ^-) is decreased with increasing the temperature. (c) The gap between two curves of $P(\sigma^+)$ and $P(\sigma^-)$ i.e., $\Delta P = P(\sigma^+) - P(\sigma^-)$, as a function of wavelength at different temperature.

4. Conclusions

In conclusion, we have studied the circular polarization resolved PL in the MoS_2/MoO_3 heterostructure. It is found that the DPs of $P(\sigma^+)$ and $P(\sigma^-)$ are unequal. This effect might come from the p-doping of MoS_2 caused by the carriers transfer between MoS_2 and MoO_3 layers due to their specific band structures. Then, built-in voltage is generated which may lead to the shift of overlaps of electron-hole distributions at the K and K′ valleys. As a result, asymmetric valley polarization is obtained, and the DPs for the right and left-handed circularly polarized PL are unequal in the MoS_2/MoO_3 heterostructure. Particularly, the MoS_2/MoO_3 heterostructure is in favor of right-handed circularly polarized PL from the K valley of MoS_2. By decreasing the temperature in the MoS_2/MoO_3 heterostructure, the difference between $P(\sigma^+)$ and $P(\sigma^-)$ is enlarged. These results are universal in MoS_2/MoO_3 heterostructures. Our investigation provides an opportunity for developing valleytronics and novel two-dimensional optoelectronic devices.

Funding

National Key R&D Program of China (2017YFA0303702); National Natural Science Foundation of China (11634005, 11674155, 61975078, 11974177, 11621091); "333 project" from Jiangsu province (BRA2016350).

Optics EXPRESS

Disclosures

The authors declare no conflicts of interest.

References

1. O. Gunawan, Y. P. Shkolnikov, K. Vakili, T. Gokmen, E. P. De Poortere, and M. Shayegan, "Valley Susceptibility of an Interacting Two-Dimensional Electron System," Phys. Rev. Lett. **97**(18), 186404 (2006).
2. A. Rycerz, J. Tworzydlo, and C. W. J. Beenakker, "Valley filter and valley valve in graphene," Nat. Phys. **3**(3), 172–175 (2007).
3. D. Xiao, W. Yao, and Q. Niu, "Valley-Contrasting Physics in Graphene: Magnetic Moment and Topological Transport," Phys. Rev. Lett. **99**(23), 236809 (2007).
4. F. Zhang, J. Jung, G. A. Fiete, Q. Niu, and A. H. MacDonald, "Spontaneous Quantum Hall States in Chirally Stacked Few-Layer Graphene Systems," Phys. Rev. Lett. **106**(15), 156801 (2011).
5. X. Xu, W. Yao, D. Xiao, and T. F. Heinz, "Spin and pseudospins in layered transition metal dichalcogenides," Nat. Phys. **10**(5), 343–350 (2014).
6. G. Kioseoglou, A. T. Hanbicki, M. Currie, A. L. Friedman, D. Gunlycke, and B. T. Jonker, "Valley polarization and intervalley scattering in monolayer MoS_2," Appl. Phys. Lett. **101**(22), 221907 (2012).
7. G. Sallen, L. Bouet, X. Marie, G. Wang, C. R. Zhu, W. P. Han, Y. Lu, P. H. Tan, T. Amand, B. L. Liu, and B. Urbaszek, "Robust optical emission polarization in MoS_2 monolayers through selective valley excitation," Phys. Rev. B **86**(8), 081301 (2012).
8. D. MacNeill, C. Heikes, K. F. Mak, Z. Anderson, and A. Kormányos, "Breaking of Valley Degeneracy by Magnetic Field in Monolayer $MoSe_2$," Phys. Rev. Lett. **114**(3), 037401 (2015).
9. F. Gao, Y. Gong, M. Titze, R. Almeida, P. M. Ajayan, and H. Li, "Valley trion dynamics in monolayer $MoSe_2$," Phys. Rev. B **94**(24), 245413 (2016).
10. Z. Sun, J. Gu, A. Ghazaryan, Z. Shotan, C. R. Considine, M. Dollar, B. Chakraborty, X. Liu, P. Ghaemi, S. K. Cohen, and V. M. Menon, "Optical control of room-temperature valley polaritons," Nat. Photonics **11**(8), 491–496 (2017).
11. J. R. Schaibley, P. Rivera, H. Yu, K. L. Seyler, J. Yan, D. G. Mandrus, T. Taniguchi, K. Watanabe, W. Yao, and X. Xu, "Directional interlayer spin-valley transfer in two-dimensional heterostructures," Nat. Commun. **7**(1), 13747 (2016).
12. L. Guo, M. Wu, T. Cao, D. M. Monahan, Y.-H. Lee, S. G. Louie, and G. R. Fleming, "Exchange-driven intravalley mixing of excitons in monolayer transition metal dichalcogenides," Nat. Phys. **15**(3), 228–232 (2019).
13. D. Xiao, G.-B. Liu, W. Feng, X. Xu, and W. Yao, "Coupled Spin and Valley Physics in Monolayers of MoS_2 and Other Group-VI Dichalcogenides," Phys. Rev. Lett. **108**(19), 196802 (2012).
14. K. F. Mak, K. L. McGill, J. Park, and P. L. McEuen, "The valley Hall effect in MoS_2 transistors," Science **344**(6191), 1489–1492 (2014).
15. K. F. Mak, K. He, J. Shan, and T. F. Heinz, "Control of valley polarization in monolayer MoS_2 by optical helicity," Nat. Nanotechnol. **7**(8), 494–498 (2012).
16. H. Zeng, J. Dai, W. Yao, D. Xiao, and X. Cui, "Valley polarization in MoS_2 monolayers by optical pumping," Nat. Nanotechnol. **7**(8), 490–493 (2012).
17. W. B. Shi, L. Zhang, D. Wang, R. L. Zhang, Y. Y. Zhu, L. H. Zhang, R. W. Peng, W. Z. Bao, R. H. Fan, and M. Wang, "Hybrid coupling enhances photoluminescence of monolayer MoS_2 on plasmonic nanostructures," Opt. Lett. **43**(17), 4128 (2018).
18. S. Zu, B. Li, Y. Gong, Z. Li, P. M. Ajayan, and Z. Fang, "Active Control of Plasmon–Exciton Coupling in MoS_2–Ag Hybrid Nanostructures," Adv. Opt. Mater. **4**(10), 1463–1469 (2016).
19. Y. Zhou, X. Hu, W. Gao, H. Song, S. Chu, H. Yang, and Q. Gong, "Photoluminescence enhancement of monolayer tungsten disulfide in complicated plasmonic microstructures," Opt. Laser Technol. **102**, 268–273 (2018).
20. L. Y. Sun, C.-Y. Wang, A. Krasnok, J. Choi, J. Shi, J. S. Gomez-Diaz, A. Zepeda, S. Gwo, C.-K. Shih, A. Alù, and X. Q. Li, "Separation of valley excitons in a MoS_2 monolayer using a subwavelength asymmetric groove array," Nat. Photonics **13**(3), 180–184 (2019).
21. Y. Li, J. Ludwig, T. Low, A. Chernikov, X. Cui, G. Arefe, Y. D. Kim, A. M. van der Zande, A. Rigosi, H. M. Hill, S. H. Kim, J. Hone, Z. Li, D. Smirnov, and T. F. Heinz, "Valley Splitting and Polarization by the Zeeman Effect in Monolayer $MoSe_2$," Phys. Rev. Lett. **113**(26), 266804 (2014).
22. J. Kim, X. Hong, C. Jin, S.-F. Shi, C.-Y. S. Chang, M.-H. Chiu, L.-J. Li, and F. Wang, "Ultrafast generation of pseudo-magnetic field for valley excitons in WSe_2 monolayers," Science **346**(6214), 1205–1208 (2014).
23. K. L. Seyler, D. Zhong, B. Huang, X. Linpeng, N. P. Wilson, T. Taniguchi, K. Watanabe, W. Yao, D. Xiao, M. A. McGuire, K.-M. C. Fu, and X. Xu, "Valley Manipulation by Optically Tuning the Magnetic Proximity Effect in WSe_2 /CrI_3 Heterostructures," Nano Lett. **18**(6), 3823–3828 (2018).
24. Y. Ye, J. Xiao, H. Wang, Z. Ye, H. Zhu, M. Zhao, Y. Wang, J. Zhao, X. Yin, and X. Zhang, "Electrical generation and control of the valley carriers in a monolayer transition metal dichalcogenide," Nat. Nanotechnol. **11**, 597–602 (2016).
25. O. L. Sanchez, D. Ovchinnikov, S. Misra, A. Allain, and A. Kis, "Valley Polarization by Spin Injection in a Light-Emitting van der Waals Heterojunction," Nano Lett. **16**(9), 5792–5797 (2016).
26. Y. J. Zhang, T. Oka, R. Suzuki, J. T. Ye, and Y. Iwasa, "Electrically Switchable Chiral Light-Emitting Transistor," Science **344**(6185), 725–728 (2014).

Optics EXPRESS

27. W. Yang, J. Shang, J. Wang, X. Shen, B. Cao, N. Peimyoo, C. Zou, Y. Chen, Y. Wang, C. Cong, W. Huang, and T. Yu, "Electrically Tunable Valley-Light Emitting Diode (vLED) Based on CVD-Grown Monolayer WS_2," Nano Lett. **16**(3), 1560–1567 (2016).
28. D. Wang, J.-N. Li, Y. Zhou, D.-H. Xu, X. Xiong, R.-W. Peng, and M. Wang, "Van der Waals epitaxy of ultrathin α-MoO_3 sheets on mica substrate with single-unit-cell thickness," Appl. Phys. Lett. **108**(5), 053107 (2016).
29. H. M. Oh, G. H. Han, H. Kim, J. J. Bae, M. S. Jeong, and Y. H. Lee, "Photochemical Reaction in Monolayer MoS_2 via Correlated Photoluminescence, Raman Spectroscopy, and Atomic Force Microscopy," ACS Nano **10**(5), 5230–5236 (2016).
30. S. Schmitt-Rink, D. S. Chemla, and D. A. B. Miller, "Theory of transient excitonic optical nonlinearities in semiconductor quantum-well structures," Phys. Rev. B **32**(10), 6601–6609 (1985).
31. X. Zhang, H. Nan, S. Xiao, X. Wan, Z. Ni, X. Gu, and K. Ostrikov, "Shape-uniform, high-quality monolayer MoS_2 crystals for gate-tunable photoluminescence," ACS Appl. Mater. Interfaces **9**(48), 42121–42130 (2017).
32. W. Bao, N. J. Borys, C. Ko, J. Suh, W. Fan, A. Thron, Y. Zhang, A. Buyanin, J. Zhang, S. Cabrini, P. D. Ashby, A. Weber-Bargioni, S. Tongay, S. Aloni, D. F. Ogletree, J. Wu, M. B. Salmeron, and P. J. Schuck, "Visualizing nanoscale excitonic relaxation properties of disordered edges and grain boundaries in monolayer molybdenum disulfide," Nat. Commun. **6**(1), 7993 (2015).
33. A. K. M. Newaz, D. Prasai, J. I. Ziegler, D. Caudel, S. Robinson, R. F. Haglund Jr., and K. I. Bolotin, "Electrical control of optical properties of monolayer MoS_2," Solid State Commun. **155**, 49–52 (2013).
34. A. J. Molina-Mendoza, J. L. Lado, J. O. Island, M. A. Niño, L. Aballe, M. Foerster, F. Y. Bruno, A. López-Moreno, L. Vaquero-Garzon, H. S. J. van der Zant, G. Rubio-Bollinger, N. Agraït, E. M. Pérez, J. Fernández-Rossier, and A. Castellanos-Gomez, "Centimeter-Scale Synthesis of Ultrathin Layered MoO_3 by van der Waals Epitaxy," Chem. Mater. **28**(11), 4042–4051 (2016).
35. P. K. Nayak, Y. Horbatenko, S. Ahn, G. Kim, J.-U. Lee, K. Y. Ma, A.-R. Jang, H. Lim, D. Kim, S. Ryu, H. Cheong, N. Park, and H. S. Shin, "Probing Evolution of Twist-Angle-Dependent Interlayer Excitons in $MoSe_2$/WSe_2 van der Waals Heterostructures," ACS Nano **11**(4), 4041–4050 (2017).
36. G. Kresse and J. Hafner, "Ab initio molecular dynamics for liquid metals," Phys. Rev. B **47**(1), 558–561 (1993).
37. G. Kresse and J. Furthmüller, "Efficient iterative schemes for ab initio total-energy calculations using a plane-wave basis set," Phys. Rev. B **54**(16), 11169–11186 (1996).
38. G. Kresse and D. Joubert, "From ultrasoft pseudopotentials to the projector augmented-wave method," Phys. Rev. B **59**(3), 1758–1775 (1999).
39. P. Hohenberg and W. Kohn, "Inhomogeneous Electron Gas," Phys. Rev. **136**(3B), B864–B871 (1964).
40. W. Kohn and L. J. Sham, "Self-Consistent Equations Including Exchange and Correlation Effects," Phys. Rev. **140**(4A), A1133–A1138 (1965).
41. H. J. Monkhorst and J. D. Pack, "Special Points for Brillouin-Zone Integration," Phys. Rev. B **13**(12), 5188–5192 (1976).
42. J. P. Perdew, K. Burke, and M. Ernzerhof, "Generalized Gradient Approximation Made Simple," Phys. Rev. Lett. **77**(18), 3865–3868 (1996).
43. The core-valence interactions are treated by the projector augmented wave (PAW) method [38], where the plane wave expansion is truncated with a cutoff energy 520 eV. We employ the exchange-correlation functional as the local density approximation (LDA) [39,40]. The convergence tolerance for the self-consistent-field iteration was set to 10^{-4} eV, and the two dimensional 3×2 Monkhorst-Pack grid in momentum space is applied [41]. To minimize the lattice mismatching effect, a p$\left(2\sqrt{3}\times 5\right)$ MoS_2 supercell and p(3×4) MoO_3 supercell were constructed into the MoS_2/MoO_3 heterostructure. To confirm this result, we also constructed a larger supercell of MoS_2/MoO_3 heterostructure with p(6×6) MoS_2 supercell and p(4×5) MoO_3 supercell. In this group of test, we employed the generalized gradient approximation (GGA) [42] as the exchange-correlation function where the two dimensional 22 Monkhorst-Pack grid in momentum space is applied [41].
44. L. Yang, K. Majumdar, H. Liu, Y. Du, H. Wu, M. Hatzistergos, P. Y. Hung, R. Tiechelmann, W. Tsai, C. Hobbs, and P. D. Ye, "Chloride Molecular Doping Technique on 2D Materials: WS_2 and MoS_2."," Nano Lett. **14**(11), 6275–6280 (2014).
45. S. Mouri, Y. Miyauchi, and K. Matsuda, "Tunable Photoluminescence of Monolayer MoS_2 via Chemical Doping," Nano Lett. **13**(12), 5944–5948 (2013).
46. Q. H. Wang, K. K. Zadeh, A. Kis, J. N. Coleman, and M. S. Strano, "Electronics and optoelectronics of two-dimensional transition metal dichalcogenides," Nat. Nanotechnol. **7**(11), 699–712 (2012).
47. A. Kormányos, V. Zólyomi, N. D. Drummond, P. Rakyta, G. Burkard, and V. I. Fal'ko, "Monolayer MoS_2: Trigonal warping, the Γ valley, and spin-orbit coupling effects," Phys. Rev. B: Condens. Matter Mater. Phys. **88**(4), 045416 (2013).
48. Z. Li, R. Ye, R. Feng, Y. Kang, X. Zhu, J. M. Tour, and Z. Fang, "Graphene Quantum Dots Doping of MoS_2 Monolayers," Adv. Mater. **27**(35), 5235–5240 (2015).
49. D. Wang, W.-B. Shi, H. Jing, R.-L. Zhang, Y. Zhu, J. Su, L.-H. Zhang, R. Peng, W. Bao, R.-H. Fan, and M. Wang, "Photon-induced carrier recombination in the non-layered-structured hybrid organic-inorganic perovskite nano-sheets," Opt. Express **26**(21), 27504 (2018).